AGU PUBLICATIONS

JGR

Journal of Geophysical Research: Space Physics

RESEARCH ARTICLE
10.1002/2017JA024027

Key Points:
- As the wave normal angle decreases, the spectral range of excited magnetosonic waves becomes broader
- For the exactly perpendicular magnetosonic waves, there is no energization in the parallel direction for both cold protons and electrons
- For magnetosonic wave with a finite parallel wave number, there is a significant energization in the parallel direction for electrons

Correspondence to:
X. Gao,
gaoxl@mail.ustc.edu.cn

Citation:
Sun, J., X. Gao, Q. Lu, L. Chen, X. Liu, X. Wang, X. Tao, and S. Wang (2017), Spectral properties and associated plasma energization by magnetosonic waves in the Earth's magnetosphere: Particle-in-cell simulations, *J. Geophys. Res. Space Physics*, *122*, 5377–5390, doi:10.1002/2017JA024027.

Received 12 FEB 2017
Accepted 3 MAY 2017
Accepted article online 8 MAY 2017
Published online 24 MAY 2017

Spectral properties and associated plasma energization by magnetosonic waves in the Earth's magnetosphere: Particle-in-cell simulations

Jicheng Sun[1,2,3], Xinliang Gao[1,2,4], Quanming Lu[1,2], Lunjin Chen[3], Xu Liu[3], Xueyi Wang[5], Xin Tao[1,2], and Shui Wang[1,2]

[1]CAS Key Laboratory of Geospace Environment, Department of Geophysics and Planetary Science, University of Science and Technology of China, Hefei, China, [2]Collaborative Innovation Center of Astronautical Science and Technology, Harbin, China, [3]Department of Physics, University of Texas at Dallas, Richardson, Texas, USA, [4]State Key Laboratory of Space Weather, Chinese Academy of Sciences, Beijing, China, [5]Physics Department, Auburn University, Auburn, Alabama, USA

Abstract In this paper, we perform a 1-D particle-in-cell (PIC) simulation model consisting of three species, cold electrons, cold ions, and energetic ion ring, to investigate spectral structures of magnetosonic waves excited by ring distribution protons in the Earth's magnetosphere, and dynamics of charged particles during the excitation of magnetosonic waves. As the wave normal angle decreases, the spectral range of excited magnetosonic waves becomes broader with upper frequency limit extending beyond the lower hybrid resonant frequency, and the discrete spectra tends to merge into a continuous one. This dependence on wave normal angle is consistent with the linear theory. The effects of magnetosonic waves on the background cold plasma populations also vary with wave normal angle. For exactly perpendicular magnetosonic waves (parallel wave number $k_{||} = 0$), there is no energization in the parallel direction for both background cold protons and electrons due to the negligible fluctuating electric field component in the parallel direction. In contrast, the perpendicular energization of background plasmas is rather significant, where cold protons follow unmagnetized motion while cold electrons follow drift motion due to wave electric fields. For magnetosonic waves with a finite $k_{||}$, there exists a nonnegligible parallel fluctuating electric field, leading to a significant and rapid energization in the parallel direction for cold electrons. These cold electrons can also be efficiently energized in the perpendicular direction due to the interaction with the magnetosonic wave fields in the perpendicular direction. However, cold protons can be only heated in the perpendicular direction, which is likely caused by the higher-order resonances with magnetosonic waves. The potential impacts of magnetosonic waves on the energization of the background cold plasmas in the Earth's inner magnetosphere are also discussed in this paper.

1. Introduction

Magnetosonic waves, also known as ion Bernstein modes, are the most common electromagnetic emissions between the proton gyrofrequency and the lower hybrid resonant frequency in the Earth's magnetosphere [*Russell et al.*, 1970; *Gurnett*, 1976; *Santolík et al.*, 2002; *Boardsen et al.*, 2014; *Tsurutani et al.*, 2014]. Magnetosonic waves play a potential role in both scattering and accelerating relativistic electrons in the Van Allen radiation belt [*Horne and Thorne*, 1998; *Horne et al.*, 2007; *Li et al.*, 2014, 2016; *Bortnik et al.*, 2015; *Chen et al.*, 2015; *Li et al.*, 2015; *Tao and Li*, 2016]. The first observation of magnetosonic waves in the Earth's magnetosphere can be traced back to the late 1960s, which was captured by the OGO 3 spacecraft [*Russell et al.*, 1969]. Since magnetosonic waves are typically detected within a few degrees near the geomagnetic equator, they are also termed as "equatorial noise" in the literature. Both observations [*Perraut et al.*, 1982; *Boardsen et al.*, 1992; *Meredith et al.*, 2008; *Ma et al.*, 2014;] and theoretical studies [*Gulelmi et al.*, 1975; *Curtis and Wu*, 1979; *McClements et al.*, 1994; *Sun et al.*, 2016a] have demonstrated that ring current ions in the Earth's inner magnetosphere with the positive phase space density gradient around the local Alfven speed in the perpendicular velocity distribution (i.e., ring-like velocity distribution) provide the free energy to excite magnetosonic waves. Magnetosonic waves can occur both inside and outside the plasmasphere, with a preferential occurrence in the afternoon sector of the plasmapause region [*Ma et al.*, 2013].

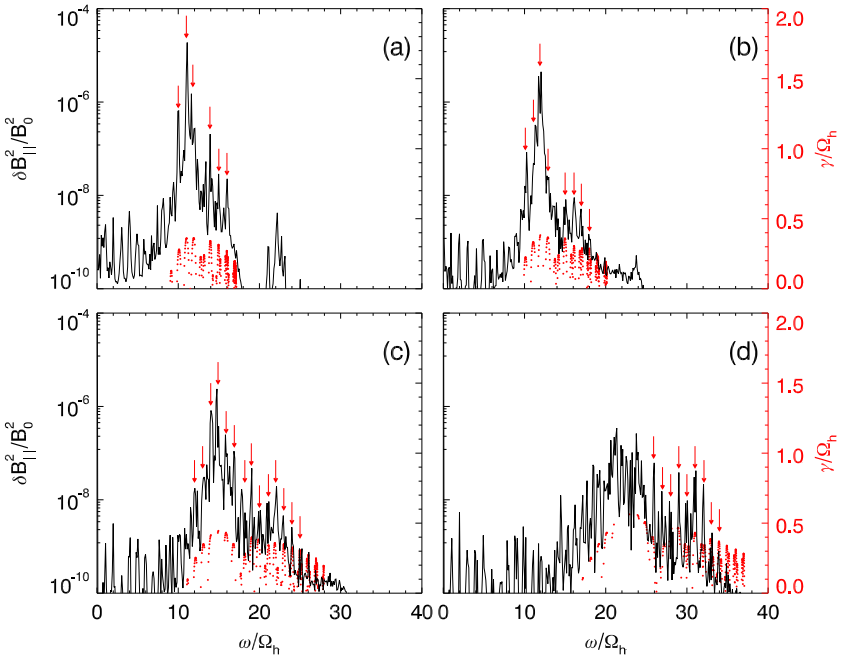

Figure 1. The power of parallel fluctuating magnetic fields $\delta B_{||}^2/B_0^2$ as a function of the normalized wave frequency ω/Ω_h for different wave normal angles: (a) $\theta = 90°$, (b) for $\theta = 89°$, (c) for $\theta = 88°$, and (d) for $\theta = 87°$. The number density of ring distribution protons $n_{hr}/n_e = 0.5\%$. The red dots in each panel denotes the growth rate γ/Ω_h calculated by the linear theory with the same parameters for each simulation. The red arrows in Figure 1 are added in line with the discrete peaks of linear growth rates.

Magnetosonic waves are generated with very large wave normal angles, meaning that their wave vectors are nearly perpendicular to the background magnetic field [*Perraut et al.*, 1982; *Boardsen et al.*, 1992]. Moreover, magnetosonic waves in the inner magnetosphere usually show up at several harmonics of the local proton gyrofrequency [*Perraut et al.*, 1982], which exhibit a discrete spectrum in the time-frequency spectrogram [*Balikhin et al.*, 2015]. However, recent observations [*Tsurutani et al.*, 2014] revealed that magnetosonic waves with the large intensity do not have a discrete spectrum in the inner magnetosphere. The discrete and continuous nature of magnetosonic wave instability has been explored through the linear theory. Based on the linear theory, two potential mechanisms have been proposed to explain the formation of the continuous spectrum of magnetosonic waves: (1) the overlapping effect of two adjacent harmonics due to a finite harmonic frequency width for a sufficiently large growth rate [*Sun et al.*, 2016a, 2016b; *Chen et al.*, 2016], which does not require a finite k_z (the wave vector component parallel to the external magnetic field), and (2) the contribution from multiple wave-particle resonant interactions for the presence of a finite k_z [*Chen*, 2015]. Particle-in-cell (PIC) simulations [*Liu et al.*, 2011; *Min and Liu*, 2015; *Sun et al.*, 2016b] have also been utilized to investigate the generation of magnetosonic waves by energetic ring distribution protons, which can further evaluate the results from the linear theory. Not only discrete magnetosonic spectra with narrow-banded emissions at harmonics of the proton gyrofrequency but also continuous magnetosonic spectra have already been successfully reproduced in previous works [*Sun et al.*, 2016a, 2016b; *Chen et al.*, 2016]. However, the influences of the wave normal angles on the spectral properties of the magnetosonic waves excited by energetic ring distribution protons, as well as on the energization of the background plasma during the evolution of the magnetosonic waves, have never been studied by PIC simulations in a self-consistent way.

In this paper we discuss, for the first time, the energization of the background cold plasma ion and electron components by magnetosonic waves based on the results from 1-D PIC simulations. We also study the effects of wave normal angles of magnetosonic waves on their spectral structures. This paper is organized as follows. The 1-D PIC simulation model and initial plasma parameters are described in section 2, followed by the simulation results in section 3. At last, the principle results and discussion are given in section 4.

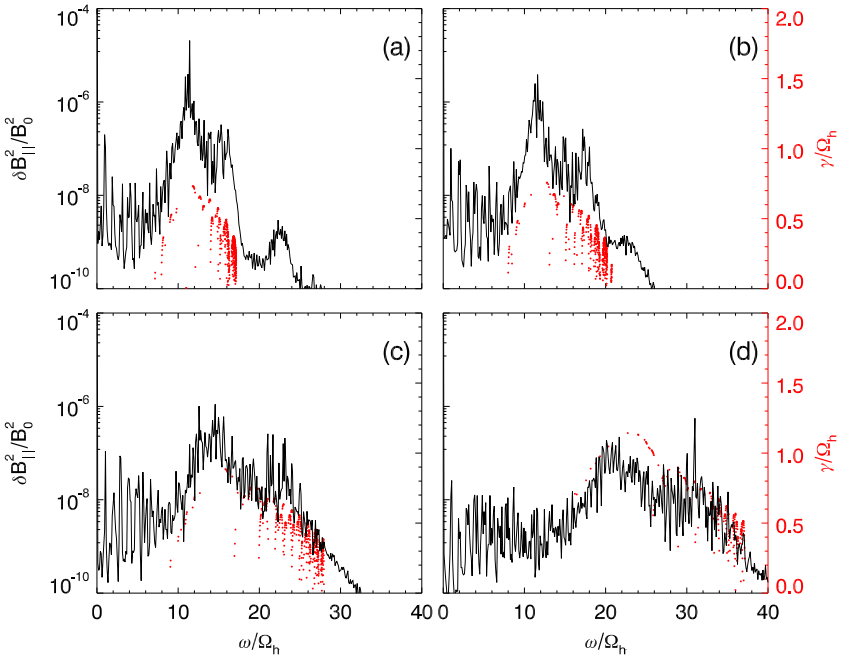

Figure 2. The same format as Figure 1 except for the number density of ring distribution protons $n_{hr}/n_e = 2\%$.

2. PIC Simulation Model

For studying spectral properties of excited MS waves and accompanying energization of background plasmas, we employ a 1-D PIC simulation model [*Sun et al.*, 2016a, 2016b]. This simulation only allows spatial variations in the x direction (i.e., wave vector direction), in a homogeneous magnetized plasma with the periodic boundary condition. The background magnetic field $\mathbf{B}_0$ lies in the x-y plane and is defined as $\mathbf{B}_0 = B_0(\cos\theta\hat{\mathbf{x}} + \sin\theta\hat{\mathbf{y}})$, where θ is the angle between wave vector and the ambient magnetic field, i.e., the wave normal angle. Therefore, we can control the wave normal angle of generated magnetosonic waves by varying the direction of the background magnetic field. The simulation model consists of three plasma components representing the thermal electrons and protons (Maxwellian velocity distributions) and a tenuous ring distribution of energetic protons, while the distribution function of ring distribution protons is given by $f_{hr} = n_{hr}\delta(v_{||})\delta(v_\perp - V_R)/(2\pi v_\perp)$, where $v_{||}$ and $v_\perp$ are velocities parallel and perpendicular to the background magnetic field, and V_R is the proton ring velocity. Hereafter, subscripts "c", "hc", and "hr" refer to cold electrons, cold protons, and ring distribution protons, respectively.

In this simulation, space and time are normalized to the proton inertial length $\lambda_i = c/\omega_{ph}$ (c and ω_{ph} are the light speed and proton plasma frequency, respectively) and the inverse of proton gyrofrequency Ω_h^{-1}, respectively. The number of grid cells is $n_x = 8192$, with a spatial resolution of $\Delta x = 7.5\times10^{-4}\lambda_i$. There are on average 60 macroparticles in every cell for each species. As shown in Figures 1 and 2, the number of macroparticles within one wavelength of dominant magnetosonic modes in our simulations is estimated to be sufficiently large (~10^4), which can reduce the numerical noise to a low level. The time step is $\Omega_h\Delta t = 2.5\times10^{-5}$ such that electron dynamics can be fully resolved. In order to improve the computational efficiency, the light speed is artificially chosen such that $c = 20\ V_A$ ($V_A = B_0/\sqrt{\mu_0 n_e m_h}$ is the Alfven speed, where n_e is the electron density), and the mass ratio of proton to electron $m_h/m_e = 1600$. For such artificial values, the lower hybrid resonant frequency ω_{lhr}, given by $\left(\frac{1}{\Omega_e\Omega_h} + \frac{1}{\omega_{ph}^2}\right)^{-1/2}$ (where Ω_e is the electron gyrofrequency), is about $18\Omega_h$. The proton ring velocity is initialized to $V_R = 1.0V_A$, while the thermal velocity of cold protons is set as $0.00635V_A$ and cold electrons have the same temperature as cold protons. The number densities of cold electrons, cold protons, and ring distribution protons are n_e, n_{hc}, and n_{hr}, respectively, and satisfy the condition $n_e = n_{hc} + n_{hr}$.

3. Simulation Results

By employing the self-consistent 1-D PIC simulation model, we examine the dependence of magnetic spectral structures on wave normal angles θ in the linear growth phase. We will consider two cases, case I and case II, with the number density of ring distribution protons n_{hr}/n_e set to 0.5% and 2%, respectively.

Figure 1 displays the power spectra of parallel fluctuating magnetic fields $\delta B_{||}^2/B_0^2$ versus the normalized wave frequency ω/Ω_h for case I with different values of wave normal angle, $\theta = 90°$ (1a), $\theta = 89°$ (1b), $\theta = 88°$ (1c), and $\theta = 87°$ (1d). The power spectrum is obtained by Fourier transforming of $\delta B_{||}/B_0$ from $\Omega_h t = 0$ to 60. The red dots in each panel denotes the growth rate γ/Ω_h calculated by the linear theory [*Umeda et al*., 2012] with the same parameters for the case I. The red arrows in Figure 1 are added to denote the discrete peaks of linear growth rates, which are also found to be consistent with the power peaks obtained from simulations. Note that only discrete parts of the profile of linear growth rates have been marked by the red arrows. For the wave normal angle θ is exactly 90°, only several discrete wave modes are excited in the system (Figure 1a), and the magnetosonic spectrum is roughly confined within the lower hybrid resonant frequency (~$18\Omega_h$). As the wave normal angle decreases, the spectral range of the excited magnetosonic waves becomes broader, and the upper limit of frequency range can extend beyond the lower hybrid frequency. For example, the frequency range is from Ω_h to $24\Omega_h$ when the wave normal angle θ = 89° (Figure 1b), while the frequency range is Ω_h and increases to $35\Omega_h$ when θ = 87° (Figure 1d). Furthermore, one can also notice a transition from a stronger and discrete spectrum into a weaker and continuous spectrum as the wave normal angle becomes farther away from 90°. Those dependences on wave normal angles can be found in both simulation and theoretical results for the following aspects.

1. As wave normal angle decreases, the growth rate as a function of wave frequency experiences a transition from a discrete profile to a more continuous one.
2. For the smaller wave normal angle, the unstable frequency range becomes broader, and the higher unstable frequency limit can extend beyond the lower hybrid resonant frequency.
3. For ring distribution, the peak growth rate occurs at $\theta = 90°$ and tends to be weaker as θ becomes smaller.

The power spectral density of parallel fluctuating magnetic fields $\delta B_{||}^2/B_0^2$ for case II is shown in Figure 2, for different wave normal angles $\theta = 90°$ (2a), $\theta = 89°$ (2b), $\theta = 88°$ (2c), and $\theta = 87°$ (2d). The red dots in each panel denotes the growth rateγ/Ω_h calculated by the linear theory with the same parameters for the case II. In comparison with Case I, the larger concentration of ring distribution protons in Case II provides more free energy to excite magnetosonic waves. The stronger instability leads to a more intense and more continuous magnetic spectrum for $\theta = 90°$ (Figure 2a) than case I (Figure 1a). The dependence on the wave normal angle (from Figure 2a to Figure 2d) is similar to case I, that is, as wave normal angle decreases, the frequency range of excited magnetosonic waves becomes broader, and wave spectrum tends to possess a continuous spectrum.

As well as affecting the wave spectral properties, changes in the wave normal angle also influence the particle dynamics. Hereafter, without loss of generality we will only present results of particle dynamics for case II where the number density of ring distribution protons $n_{hr}/n_e = 2\%$. Figures 3a and 3b illustrate the electron velocity distribution at $\Omega_h t = 0$ and 50, respectively, in the case of $\theta = 90°$, while Figure 3c displays the time evolution of perpendicular and parallel kinetic energies of cold electrons. Figures 3d–3f show results for ring distribution protons, and Figures 3g–3i for cold protons using the same format as Figures 3a–3c. Here the kinetic energies have been normalized by the initial value for each species. It is worth noting that for ring distribution protons, only perpendicular kinetic energy is plotted in Figure 3f due to their negligible parallel kinetic energy. For cold electrons, at $\Omega_h t = 0$, their velocity distribution satisfies a Maxwellian distribution with a peak at the thermal velocity (~$0.25V_A$) in Figure 3a. After the generation of magnetosonic waves ($\Omega_h t = 50$), it is clearly shown that the velocity distribution of cold electrons becomes broader, and a considerable part of cold electrons have gained a significant energization (Figure 3b). Further analysis shows that cold electrons are mainly energized in the perpendicular direction (Figure 3c), whose kinetic energy is increased to about 10 times of the initial value at $\Omega_h t$~0, while there is no appreciable change in their parallel energy. Similarly, background cold protons are also observed to be efficiently energized in the perpendicular direction with the maximum kinetic energy as ~60 times of their initial value (Figure 3i) but no change in their parallel energy. For hot ring distribution protons, they lose a fraction of the kinetic energy to excite magnetosonic waves (Figure 3f) and

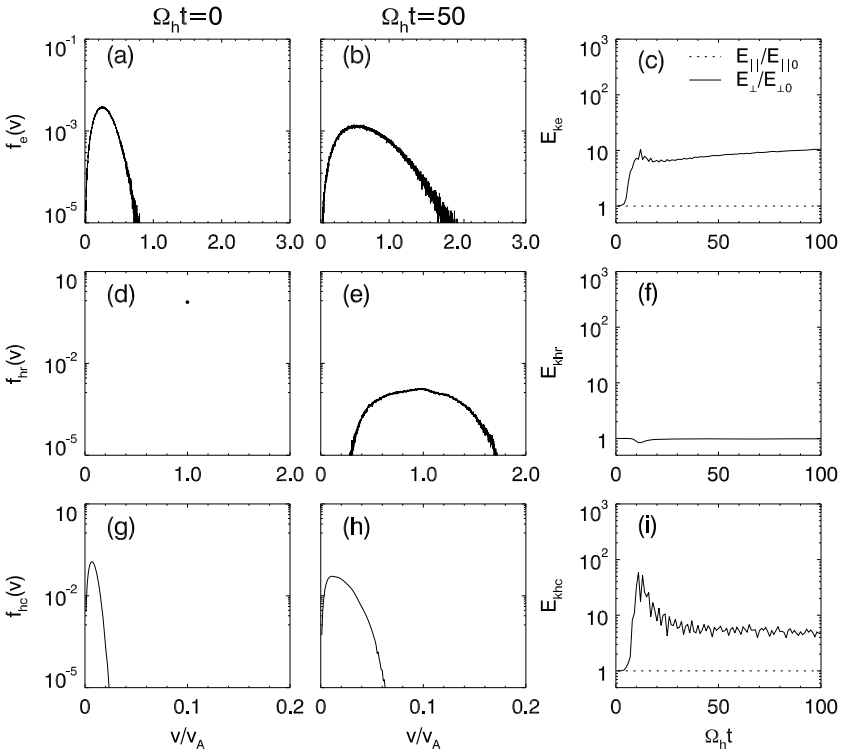

Figure 3. The electron velocity distributions for $\theta = 90°$ case at (a) $\Omega_h t = 0$ and (b) $\Omega_h t = 50$, and (c) the time profile of electron kinetic energy; (d–f) for ring distribution protons and (g–i) for cold protons. The solid and dotted lines in the third column denote perpendicular and parallel kinetic energy, respectively.

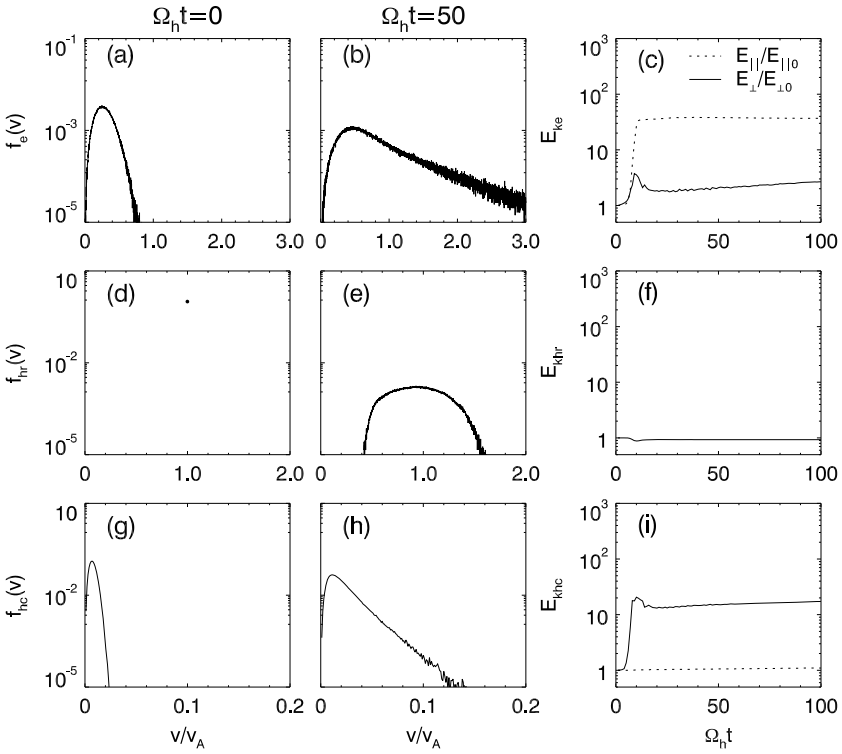

Figure 4. The same format as Figure 3 except for the wave normal angle $\theta = 88°$.

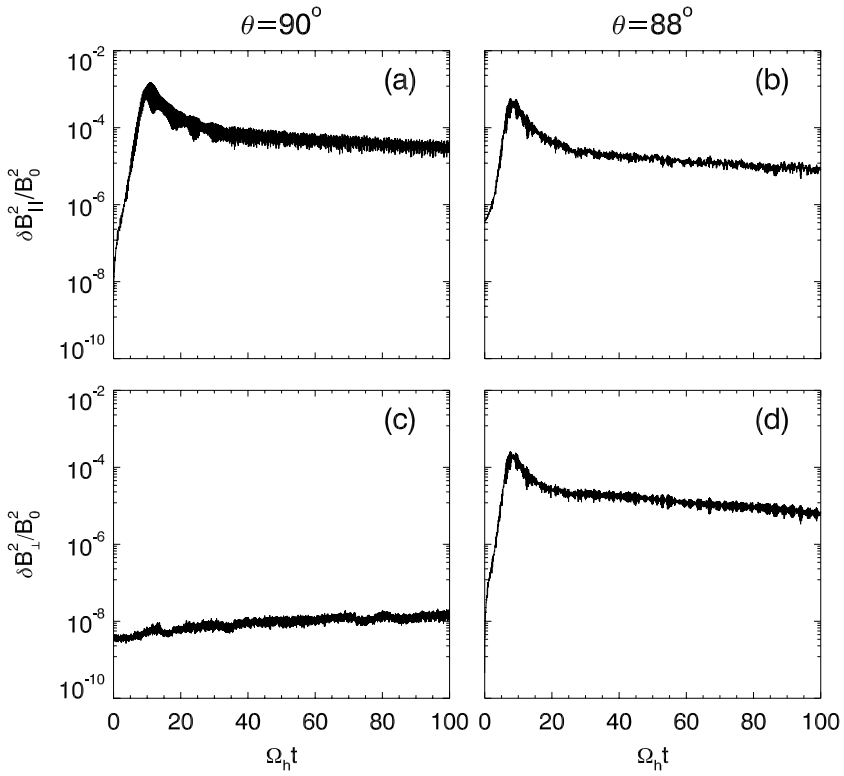

Figure 5. Time evolution of spatially averaged parallel and perpendicular fluctuating magnetic fields for both (a, c) $\theta = 90°$ and (b, d) $\theta = 88°$ cases.

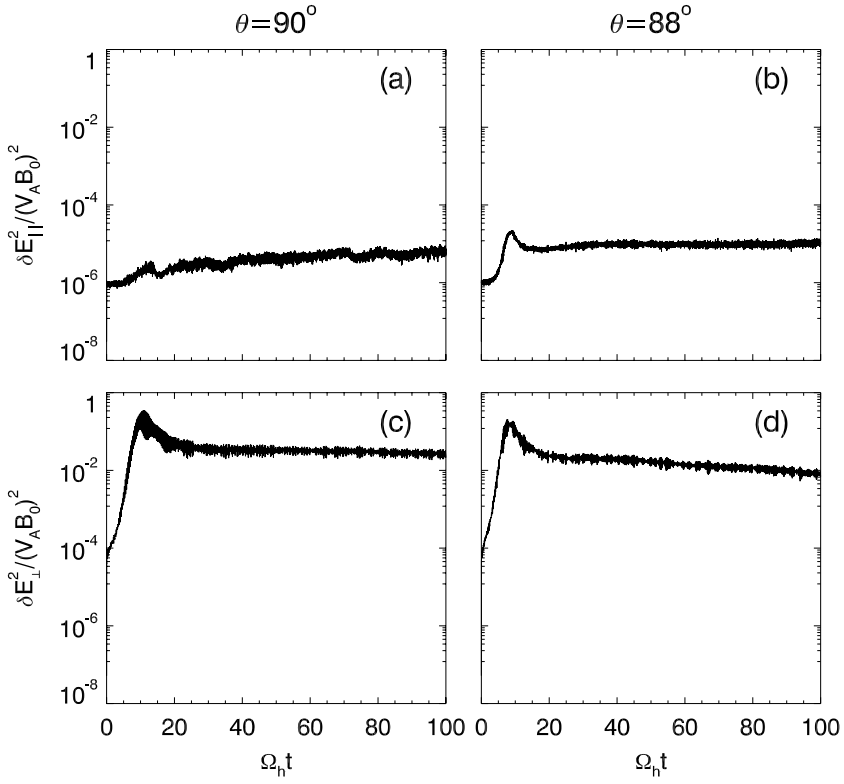

Figure 6. Time evolution of spatially averaged parallel and perpendicular fluctuating electric fields for both (a, c) $\theta = 90°$ and (b, d) $\theta = 88°$ cases.

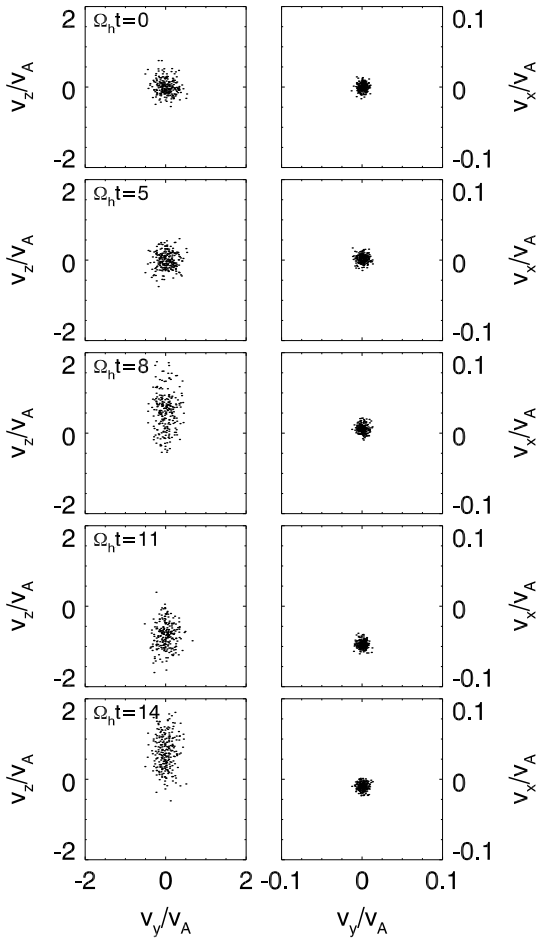

Figure 7. The scatterplots of background cold electrons in the (left column) (v_y,v_z) space and protons in the (right column) (v_y,v_x) space at $\Omega_h t$=0, 5, 8, 11, and 14, respectively, for the case of $\theta = 90°$.

experience subsequent scattering in perpendicular direction, leading to a transition from ideal ring distribution at $\Omega_h t$ = 0 (Figure 3d) into a spread ring distribution at $\Omega_h t$ = 50 (Figure 3e).

Figure 4 presents the particle velocity distribution for a smaller wave normal angle $\theta = 88°$ with the same format as that of Figure 3 (θ = 90°). In comparison with Figure 3 (θ = 90°), background cold electrons gain more energization during the generation of magnetosonic waves, which results in a broader velocity distribution (Figure 4b). More interestingly, background cold electrons are efficiently energized not only in the perpendicular direction but also predominantly in the parallel direction. As shown in Figure 4c, the parallel kinetic energy of background cold electrons increases rapidly by a factor of ~40 within $12\Omega_h^{-1}$, which is closely correlated with the growth of magnetosonic waves (Figure 6). For background cold protons, there is only perpendicular energization observed in Figure 4i but no parallel energization. Their velocity distribution becomes much broader (Figure 4h) than that of θ = 90° (Figure 3h), meaning that part of cold protons have been accelerated to much higher energies. Just as expected, ring distribution protons lose a fraction of the kinetic energy to excite magnetosonic waves (Figure 4f), and their velocity distribution is scattered into a spread ring (Figure 4e).

In order to further investigate the energization mechanism of background plasmas, we at first show the polarization properties of excited magnetosonic waves with different normal angles. Figure 5 displays the time evolution of fluctuating magnetic fields in both perpendicular and parallel directions for the wave normal angle $\theta = 90°$ (a, c) and $\theta = 88°$ (b, d), respectively. Here we only consider the linear growth phase ($<12\Omega_h^{-1}$) of the magnetosonic instability, when the efficient energization of background plasmas occurs. In the case of $\theta = 90°$, there only exists the parallel fluctuating magnetic fields in the system and the perpendicular magnetic field amplitude is in the background noise level, while in the case of $\theta = 88°$, both parallel and perpendicular fluctuating magnetic fields are clearly present with comparable amplitudes. Fluctuating electric fields are illustrated in Figure 6 for the wave normal angle $\theta = 90°$ (a, c) and $\theta = 88°$ (b, d), respectively. For both cases, the perpendicular fluctuating electric fields (Figures 6c and 6d) rapidly increase to a saturation level during the linear growth phase. A difference between the two cases is that appreciable parallel fluctuating electric fields can only be found in the case of $\theta = 88°$, while in the case of $\theta = 90°$, the parallel fluctuating electric fields remain in the noise level.

The simulation results of particle dynamics for $\theta = 90°$ are analyzed in Figures 7–9. Figure 7 shows scatterplots of background cold electrons (left column) in the (v_y,v_z) space and protons (right column) in the (v_y,v_x) space within a narrow region from $x = 1.0V_A/\Omega_h$ to $1.003V_A/\Omega_h$ at $\Omega_h t$= 0, 5, 8, 11, and 14, for the case of $\theta = 90°$.

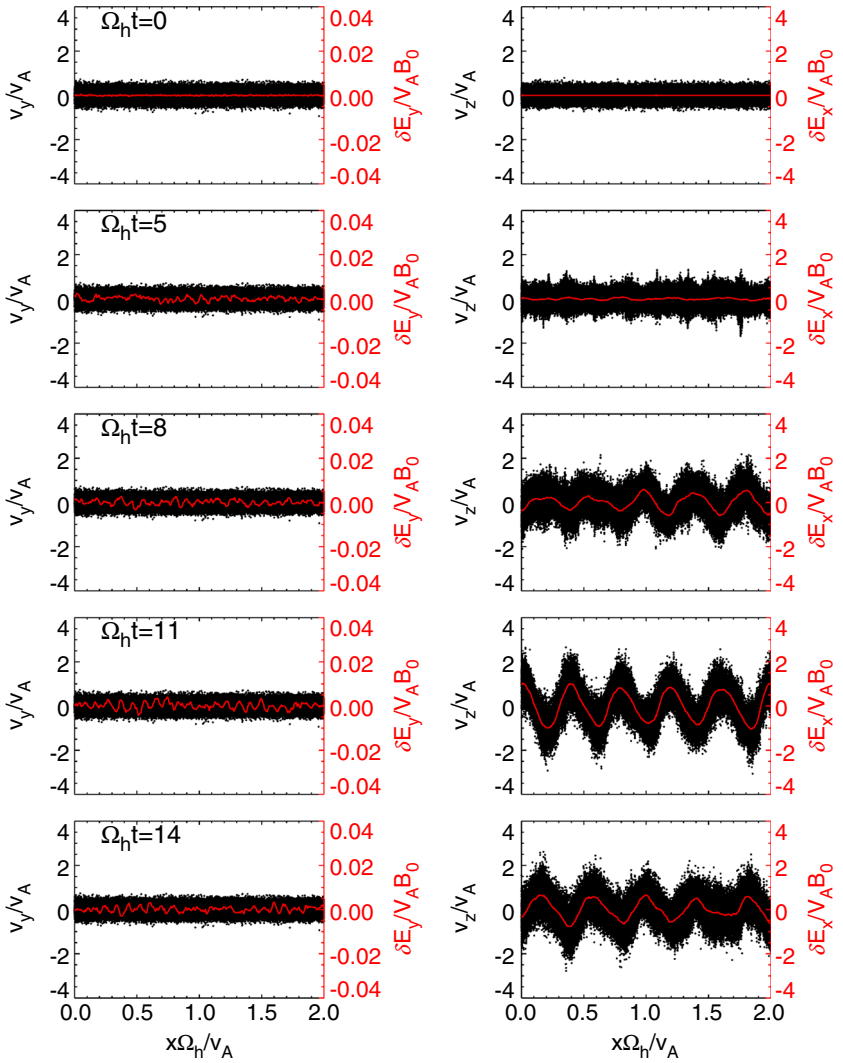

Figure 8. The scatterplots of background cold electrons in the (x,v_y) and (x,v_z) space at $\Omega_h t$=0, 5, 8, 11, and 14, respectively, in the case of $\theta = 90°$. The red lines are the (left column) spatial profiles of parallel electric field and (right column) x direction of the perpendicular electric field at corresponding times, respectively.

During the evolution of magnetosonic waves, the velocity distributions of both background electrons and protons experience little change in the parallel direction (y direction). Their velocity distributions exhibit some fluctuations in the perpendicular bulk velocity, with only a weak spread for cold electrons and almost no spread for cold protons in the perpendicular direction. This indicates the perpendicular energization shown in Figures 3c and 3i represents the fluctuation of bulk velocities associated with the excited magnetosonic waves instead of the real heating associated with the increase of thermal kinetic energy.

The dynamics of thermal electrons can be interpreted as a combination of thermal motion and bulk velocity fluctuation, the latter of which is caused by drift motion due to wave electric field. Such interpretation is demonstrated by scatterplots of background cold electrons (Figure 8) in the (x,v_y) and (x,v_z) space at $\Omega_h t$= 0, 5, 8, 11, and 14. The spatial profiles of parallel and dominant perpendicular electric fields are also overplotted by red lines in Figure 8 (left and right columns), respectively. Since both background cold electrons and protons experience similarly strong perpendicular energization but little parallel energization shown in Figure 3, we only show the results for cold electrons (Figure 8) in detail. As shown in Figure 8, on one hand, the parallel velocity distribution of electrons remains unchanged during the entire simulation due to the lack of parallel wave electric fields in the case of $\theta = 90°$. On the other hand, as the time goes on, the intensity of

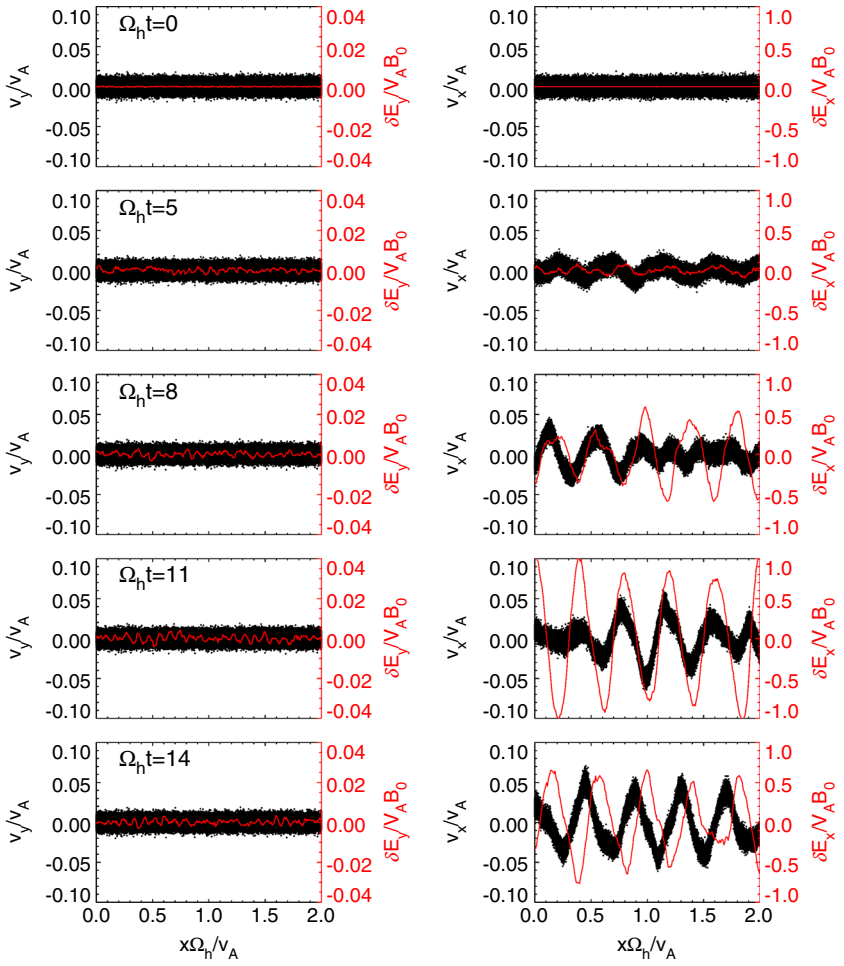

Figure 9. The same format as Figure 8 except for background cold protons.

perpendicular fluctuating electric fields begins to increase within the linear growth phase, and so does the fluctuation of the electron perpendicular bulk velocity. Moreover, both the temporal variation of amplitude and the spatial profile of fluctuations in the perpendicular bulk velocity are closely correlated with those of perpendicular fluctuating electric fields. The fluctuation of the electron bulk velocity, mostly along z direction, matches the drift velocity evaluated by the x component (the dominant component) of instantaneous electric fields (Figure 8, right column).

The dynamics of thermal protons (shown in Figure 7) can be interpreted as the combination of thermal motion and the bulk motion. For the excited waves whose frequency is much greater than proton gyrofrequency, the bulk velocity of thermal protons essentially follows unmagnetized motion. Figure 9 shows scatterplot of thermal protons in the (x,v_y) and (x,v_x) space. One can see the 90° phase difference between variation of x component of bulk velocity and x component (dominant component) of electric field at $\Omega_h t$= 14 when the waves are excited. This phase difference is consistent with unmagnetized proton motion.

The simulation results of particle dynamics for $\theta = 88°$ are shown in Figures 10–12. In order to compare with the case of $\theta = 90°$, we have transformed the simulation coordinate system to the field-aligned coordinate, where the background magnetic field $\mathbf{B}_0$ is along the y direction and the wave vector $\mathbf{k}$ lies in x-y plane. Figure 10 presents scatterplots for the case of $\theta = 88°$ using the same format as Figure 7. Initially, at $\Omega_h t = 0$, both cold electrons and protons satisfy a Maxwellian distribution. Just after the excitation of magnetosonic waves ($\Omega_h t = 9$), the cold electrons are strongly scattered in the parallel direction, but there is no significant heating in the perpendicular direction. This seems contradictory to the apparent perpendicular energization of cold electrons shown in Figure 4c. The explanation is that the perpendicular energization of cold electrons

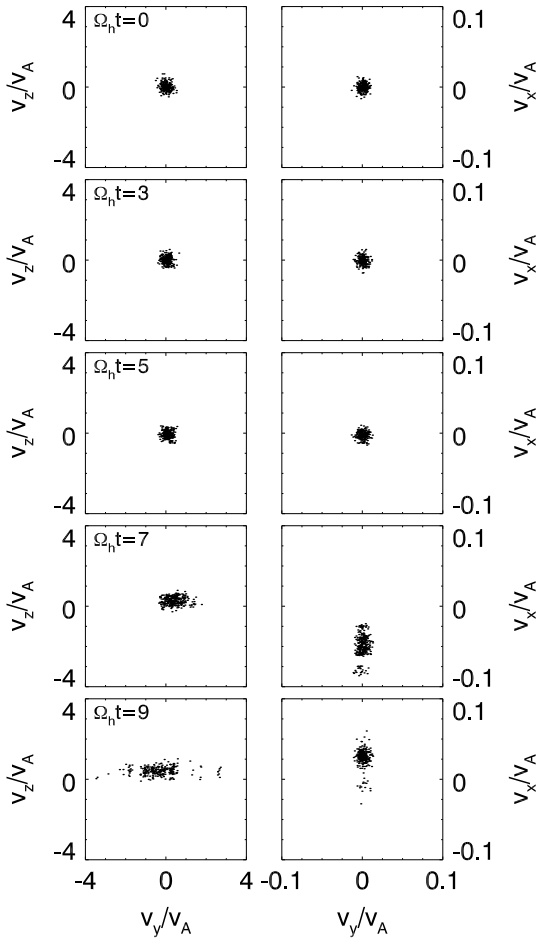

Figure 10. The scatterplots of (left column) background cold electrons in the (v_y,v_z) space and (right column) protons in the (v_y,v_x) space at $\Omega_h t$= 0, 3, 5, 7, and 9 for the case of $\theta = 88°$.

is actually the drift bulk velocity caused by the electric field of magnetosonic waves, as one can see the fluctuation of perpendicular bulk velocity (as shown in Figure 8). In contrast to the results of $\theta = 90^{\circ}$, the parallel heating of cold electrons is clearly seen in the case of $\theta = 88^{\circ}$, which is caused by the nonnegligible fluctuating parallel electric fields (Figure 6). Unlike cold electrons, the cold protons experience real perpendicular heating, leading to the broadening of velocity distribution in the perpendicular direction (Figure 10, right column).

Figure 11 further shows scatterplots of background cold electrons in the (x,v_y) and (x,v_z) space at $\Omega_h t$=0, 3, 5, 7, and 9. The spatial profiles of parallel and perpendicular electric fields are also overplotted in Figure 11 (left and right columns), respectively, which are denoted by red lines. Initially ($\Omega_h t = 0$), the cold electrons are placed uniformly along the x axis, and they do not have any fluctuation in the bulk velocity. As the time goes on (from $\Omega_h t = 0$ to $\Omega_h t = 7$), both parallel and perpendicular electric fields begin to increase, which drives fluctuations of the bulk velocity of cold electrons in both parallel and perpendicular directions. One can see that both the temporal variation of the amplitude and spatial profile of fluctuations in the bulk velocity are closely correlated with those of fluctuating electric fields. At $\Omega_h t = 9$, the electron velocity distribution gains a substantial spread in the parallel direction, which is more likely due to the phase mixing caused by the dispersive magnetosonic waves. Figure 12 provides scatterplots of background cold protons using the same format as Figure 11. Due to much heavier mass, the cold protons experience little changes in the parallel energy even when the parallel electric fields grow to the saturated amplitude (Figure 12, left column). For the perpendicular direction, some protons seem to be trapped by the wave potential and then are accelerated to a large velocity (Figure 12, right column). Here the higher-order resonances are the most promising mechanism taking effect during the perpendicular energization of cold protons. The resonant protons should satisfy $v_{||n,\,\mathrm{res}} = (\omega - n\Omega_h)/k_{||}$, where ω is the frequency of magnetosonic waves, $k_{||}$ denotes the parallel wave number, n is the orders of harmonic resonances, and $v_{||n,\,\mathrm{res}}$ is the required resonant velocity. Although the parallel wave number is very small in the case of $\theta = 88°$, the magnetosonic wave frequency is quite close to harmonics of the proton gyrofrequency, i.e., $\omega - n\Omega_h$ is also a quite small value. Therefore, the resonant velocity can be reduced to a sufficiently small value, which enables harmonic resonances between cold protons and excited magnetosonic waves.

4. Conclusions and Discussion

With a 1-D PIC simulation model, we have investigated both spectral properties and plasma energization during the generation of magnetosonic waves by ring distribution protons. Our study provides interesting

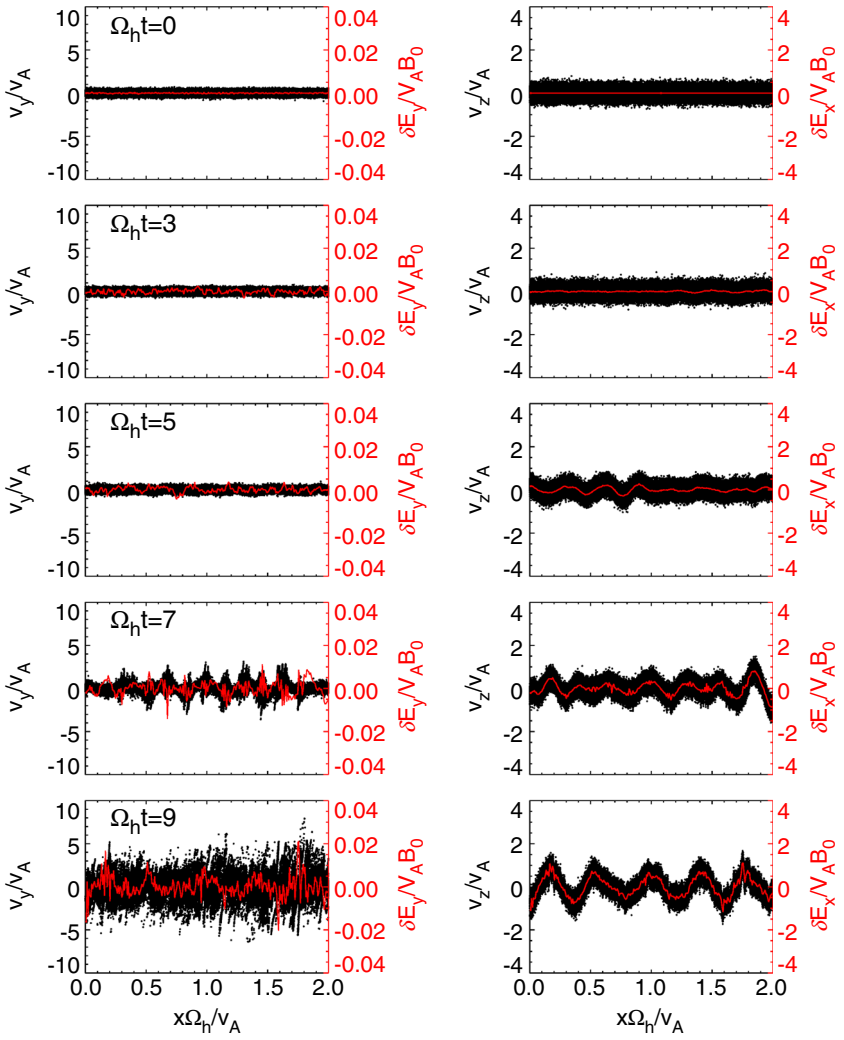

Figure 11. The scatterplots of background cold electrons in the (x,v_y) and (x,v_z) space at $\Omega_h t$=0, 3, 5, 7, and 9, respectively, in the case of $\theta = 88°$. The red lines are the spatial profile of (left column) parallel electric field and (right column) x direction of the perpendicular electric field at corresponding time.

insight into the potential impact of magnetosonic waves on background cold plasmas in the Earth's inner magnetosphere. The principal results are summarized as follows:

1. As the wave normal angle decreases, the spectral range of excited magnetosonic waves becomes broader and the upper frequency limit may even extend beyond the lower hybrid resonant frequency. For decreasing wave normal angle, the discrete spectra tend to merge into a continuous one. These results are consistent with the prediction from the linear theory [*Chen*, 2015].
2. For the exactly perpendicular magnetosonic waves, there is no energization in the parallel direction for both background cold protons and electrons due to the negligible fluctuating electric field in the parallel direction. For the perpendicular direction, thermal electrons and protons are subject to bulk motions due to wave electric field; electrons follow drift motion due to instantaneous wave electric field while protons follow unmagnetized motion.
3. For magnetosonic wave with a finite parallel wave number, there exists a nonnegligible fluctuating parallel electric field, which results in a rapid and significant energization in the parallel direction for cold electrons. At the same time, cold electrons can also be efficiently energized in the perpendicular direction due to the coupling with the magnetosonic wave fields. However, cold protons can only be heated in the perpendicular direction, which is likely caused by the higher-order resonances with magnetosonic waves.

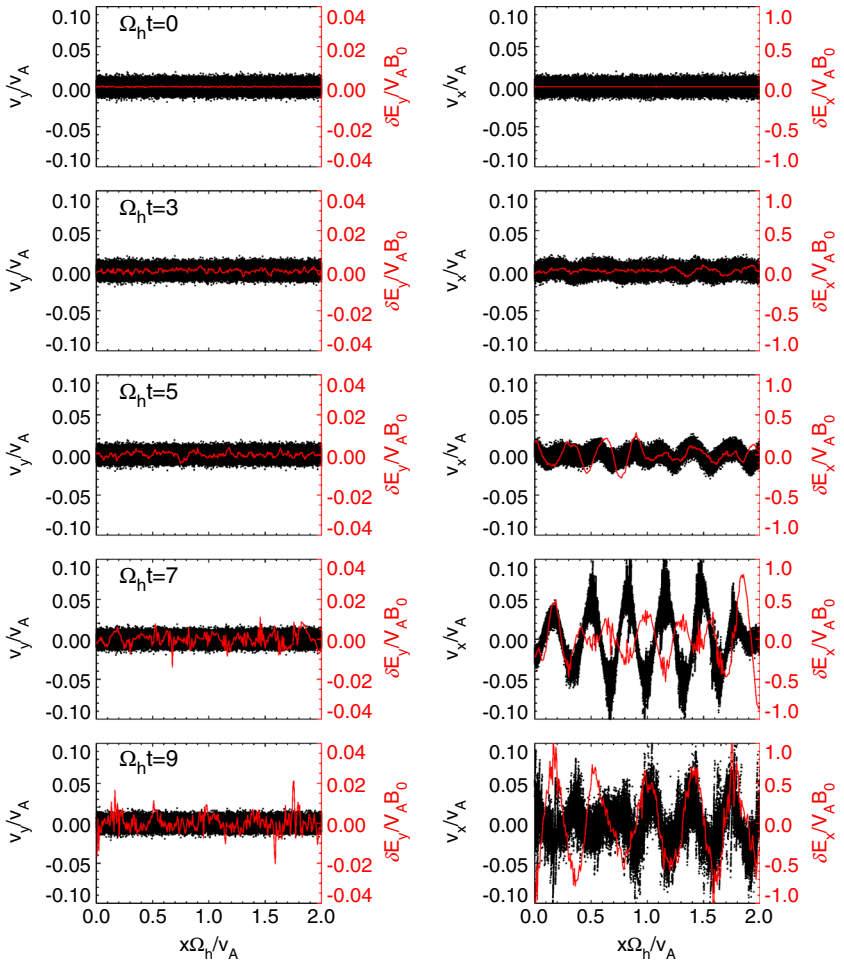

Figure 12. The same format as Figure 11 except for background cold protons.

Based on the quasi-linear theory, magnetosonic waves have been proposed to play a potential role in accelerating hot electrons via the bounce resonance [*Li et al.*, 2015, *Tao and Li*, 2016] and scattering relativistic electrons through the transit scattering [*Bortnik and Thorne*, 2010]. However, the effects of magnetosonic waves on background cold plasmas have never been reported. In this paper, with a 1-D PIC simulation model, we find that both cold electrons and protons can be efficiently energized during the generation of magnetosonic waves. In the real Earth's magnetosphere, background cold electrons are typically very cold (< ~10 eV), which are beyond the capability of plasma instruments onboard satellites. However, according to our results, both cold electrons can be energized along with the excitation of magnetosonic waves, which may enable background cold electrons to become visible for plasma detectors. Magnetosonic waves are also capable of heating cold protons in the perpendicular direction, resulting in the enhancement of fluxes of low-energy (<~100 eV) ion measurements [e.g., *Olsen et al.*, 1987]. Conversion from normalized parameters in our simulations to real magnetospheric parameters can be done to interpret heating of cold plasma due to equatorial magnetosonic waves. By adopting the background magnetic field 200 nT (at $L \approx 5$), and the plasma density = 12 cm^{-3}, we can estimate the initial kinetic energies of background cold plasmas to be less than 10 eV with the peak at ~1 eV. Soon after the saturation of magnetosonic instabilities, both cold electrons and protons are efficiently energized as shown in Figures 3b, 3e, and 3h and 4b, 4e, and 4h. The majority of cold protons and electrons can gain more than 10 times their initial kinetic energies, and some charged particles even have been accelerated up to more than 100 eV. Besides, since cold protons are preferentially energized in the perpendicular direction, so the enhanced flux of low-energy protons should peak at relatively large pitch angles [e.g., *Olsen et al.*, 1987]. However, along with the occurrence of magnetosonic waves with

wave normal angles away from 90°, the dominant energization of cold electrons occurs in the parallel direction. Therefore, we expect the enhanced flux of low-energy electrons preferentially has relatively small pitch angles. These predictions can be checked against Van Allen Probes observation, which is left as a future work.

The magnetic fluctuations generated by a proton ring in our simulations are magnetosonic waves, which has been reported in many previous works [*Liu et al*., 2011; *Chen*, 2015; *Min and Liu*, 2015; *Chen et al*., 2016; *Sun et al*., 2016a, 2016b]. Both the frequency (Figures 1 and 2) and polarization (Figures 5 and 6) of magnetic fluctuations are also consistent with properties of magnetosonic waves. Besides, the red arrows added in Figure 1 in line with the discrete peaks of linear growth rates are also found to be consistent with the power peaks obtained from simulations. However, some distinct magnetosonic wave modes, which are not expected by the linear theory, may be caused by some nonlinear process, but this is beyond the scope of this paper and left as a future work.

Acknowledgments
The work at USTC was supported by the NSFC (National Natural Science Foundation of China) grants 41474125, 41331067, 41527804, 11235009, and 41474142; Fundamental Research Funds for the Central Universities, Specialized Research Fund for State Key Laboratories, and Youth Innovation Promotion Association of Chinese Academy of Sciences (2016395). L.C. and X.L. acknowledge the support of NSF (National Science Foundation) grant AGS-1405041. The simulation data will be preserved on a long-term storage system and will be made available upon request to the corresponding author.

References

Balikhin, M. A., Y. Y. Shprits, S. N. Walker, L. Chen, N. Cornilleau-Wehrlin, I. Dandouras, O. Santolik, C. Carr, K. H. Yearby, and B. Weiss (2015), Observations of discrete harmonics emerging from equatorial noise, *Nat. Commun.*, *6*, 7703, doi:10.1038/ncomms8703.

Boardsen, S. A., D. L. Gallagher, D. A. Gurnett, W. K. Peterson, and J. L. Green (1992), Funnel-shaped, low-frequency equatorial waves, *J. Geophys. Res.*, *97*, 14,967–14,976, doi:10.1029/92JA00827.

Boardsen, S. A., G. B. Hospodarsky, C. A. Kletzing, R. F. Pfaff, W. S. Kurth, J. R. Wygant, and E. A. MacDonald (2014), Van Allen probe observations of periodic rising frequencies of the fast magnetosonic mode, *Geophys. Res. Lett.*, *41*, 8161–8168, doi:10.1002/2014GL062020.

Bortnik, J., and R. M. Thorne (2010), Transit time scattering of energetic electrons due to equatorially confined magnetosonic waves, *J. Geophys. Res.*, *115*, A07213, doi:10.1029/2010JA015283.

Bortnik, J., R. M. Thorne, B. Ni, and J. Li (2015), Analytical approximation of transit time scattering due to magnetosonic waves, *Geophys. Res. Lett.*, *42*, 1318–1325, doi:10.1002/2014GL062710.

Chen, L. (2015), Wave normal angle and frequency characteristics of magnetosonic wave linear instability, *Geophys. Res. Lett.*, *42*, 4709–4715, doi:10.1002/2015GL064237.

Chen, L., A. Maldonado, J. Bortnik, R. M. Thorne, J. Li, L. Dai, and X. Zhan (2015), Nonlinear bounce resonances between magnetosonic waves and equatorially mirroring electrons, *J. Geophys. Res. Space Physics*, *120*, 6514–6527, doi:10.1002/2015JA021174.

Chen, L., J. Sun, Q. Lu, X. Gao, Z. Xia, and Z. Zhima (2016), Generation of magnetosonic waves over a continuous spectrum, *J. Geophys. Res. Space Physics*, *121*, 1137–1147, doi:10.1002/2015JA022089.

Curtis, S. A., and C. S. Wu (1979), Gyroharmonic emissions induced by energetic ions in the equatorial plasmasphere, *J. Geophys. Res.*, *84*, 2597–2607, doi:10.1029/JA084iA06p02597.

Gulelmi, A. V., B. I. Klaine, and A. S. Potapov (1975), Excitation of magnetosonic waves with discrete spectrum in the equatorial vicinity of the plasmapause, *Planet. Space Sci.*, *23*, 279–286, doi:10.1016/0032-0633(75)90133-6.

Gurnett, D. A. (1976), Plasma wave interactions with energetic ions near the magnetic equator, *J. Geophys. Res.*, *81*, 2765–2770, doi:10.1029/JA081i016p02765.

Horne, R. B., and R. M. Thorne (1998), Potential waves for relativistic electron scattering and stochastic acceleration during magnetic storms, *Geophys. Res. Lett.*, *25*(15), 3011–3014.

Horne, R. B., R. M. Thorne, S. A. Glauert, N. P. Meredith, D. Pokhotelov, and O. Santolík (2007), Electron acceleration in the Van Allen radiation belts by fast magnetosonic waves, *Geophys. Res. Lett.*, *34*, L17107, doi:10.1029/2007GL030267.

Li, J., et al. (2014), Interactions between magnetosonic waves and radiation belt electrons: Comparisons of quasi-linear calculations with test particle simulations, *Geophys. Res. Lett.*, *41*, 4828–4834, doi:10.1002/2014GL060461.

Li, J., et al. (2016), Ultrarelativistic electron butterfly distributions created by parallel acceleration due to magnetosonic waves, *J. Geophys. Res. Space Physics*, *121*, 3212–3222, doi:10.1002/2016JA022370.

Li, X., X. Tao, Q. Lu, and L. Dai (2015), Bounce resonance diffusion coefficients for spatially confined waves, *Geophys. Res. Lett.*, *42*, 9591–9599, doi:10.1002/2015GL066324.

Liu, K., S. P. Gary, and D. Winske (2011), Excitation of magnetosonic waves in the terrestrial magnetosphere: Particle-in-cell simulations, *J. Geophys. Res.*, *116*, A07212, doi:10.1029/2010JA016372.

Ma, Q., W. Li, R. M. Thorne, and V. Angelopoulos (2013), Global distribution of equatorial magnetosonic waves observed by THEMIS, *Geophys. Res. Lett.*, *40*, 1895–1901, doi:10.1002/grl.50434.

Ma, Q., W. Li, L. Chen, R. M. Thorne, and V. Angelopoulos (2014), Magnetosonic wave excitation by ion ring distributions in the Earth's inner magnetosphere, *J. Geophys. Res. Space Physics*, *119*, 844–852, doi:10.1002/2013JA019591.

McClements, K. G., R. O. Dendy, and C. N. Lashmore-Davies (1994), A model for the generation of obliquely propagating ULF waves near the magnetic equator, *J. Geophys. Res.*, *99*(A12), 23,685–23,693, doi:10.1029/94JA01979.

Meredith, N. P., R. B. Horne, and R. R. Anderson (2008), Survey of magnetosonic waves and proton ring distributions in the Earth's inner magnetosphere, *J. Geophys. Res.*, *113*, A06213, doi:10.1029/2007JA012975.

Min, K., and K. Liu (2015), Fast magnetosonic waves driven by shell velocity distributions, *J. Geophys. Res. Space Physics*, *120*, 2739–2753, doi:10.1002/(ISSN)2169-9402.

Olsen, R. C., S. D. Shawhan, D. L. Gallagher, J. L. Green, C. R. Chappell, and P. R. Anderson (1987), Plasma observations at the Earth's magnetic equator, *J. Geophys. Res.*, *92*, 2385.

Perraut, S., A. Roux, P. Robert, R. Gendrin, J. Sauvaud, J. Bosqued, G. Kremser, and A. Korth (1982), A systematic study of ULF waves above F/H+ from GEOS 1 and 2 measurements and their relationships with proton ring distributions, *J. Geophys. Res.*, *87*, 6219–6236, doi:10.1029/JA087iA08p06219.

Russell, C. T., R. E. Holzer, and E. J. Smith (1969), OGO 3 observations of ELF noise in the magnetosphere. 1. Spatial extent and frequency of occurrence, *J. Geophys. Res.*, *74*, 755–777, doi:10.1029/JA074i003p00755.

Russell, C. T., R. E. Holzer, and E. J. Smith (1970), OGO 3 observations of ELF noise in the magnetosphere. 2. The nature of the equatorial noise, *J. Geophys. Res.*, *75*, 755–768, doi:10.1029/JA075i004p00755.

Santolík, O., J. S. Pickett, D. A. Gurnett, M. Maksimovic, and N. Cornilleau-Wehrlin (2002), Spatiotemporal variability and propagation of equatorial noise observed by Cluster, *J. Geophys. Res.*, *107*(A12), 1495, doi:10.1029/2001JA009159.

Sun, J., X. Gao, L. Chen, Q. Lu, X. Tao, and S. Wang (2016a), A parametric study for the generation of ion Bernstein modes from a discrete spectrum to a continuous one in the inner magnetosphere. I. Linear theory, *Phys. Plasmas*, *2*, 022901, doi:10.1063/1.4941283.

Sun, J., X. Gao, Q. Lu, L. Chen, X. Tao, and S. Wang (2016b), A parametric study for the generation of ion Bernstein modes from a discrete spectrum to a continuous one in the inner magnetosphere. II. Particle-in-cell simulations, *Phys. Plasmas*, *23*(2), 022902), doi:10.1063/1.4941284.

Tao, X., and X. Li (2016), Theoretical bounce resonance diffusion coefficient for waves generated near the equatorial plane, *Geophys. Res. Lett.*, *43*, 7389–7397, doi:10.1002/2016GL070139.

Tsurutani, B. T., B. J. Falkowski, J. S. Pickett, O. P. Verkhoglyadova, O. Santolik, and G. S. Lakhina (2014), Extremely intense ELF magnetosonic waves: A survey of polar observations, *J. Geophys. Res. Space Physics*, *119*, 964–977, doi:10.1002/2013JA019284.

Umeda, T., S. Matsukiyo, T. Amano, and Y. Miyoshi (2012), A numerical electromagnetic linear dispersion relation for Maxwellian ring-beam velocity distributions, *Phys. Plasmas*, *19*, 072107, doi:10.1063/1.4736848.